AIP | Applied Physics Letters

Excitation of terahertz plasmon-polariton in a grating coupled two-dimensional electron gas with a Fabry-Pérot cavity

Yongdan Huang, Hua Qin, Baoshun Zhang, Jingbo Wu, Gaochao Zhou, and Biaobing Jin

Citation: Applied Physics Letters **102**, 253106 (2013); doi: 10.1063/1.4812359
View online: http://dx.doi.org/10.1063/1.4812359
View Table of Contents: http://scitation.aip.org/content/aip/journal/apl/102/25?ver=pdfcov
Published by the AIP Publishing

Excitation of terahertz plasmon-polariton in a grating coupled two-dimensional electron gas with a Fabry-Pérot cavity

Yongdan Huang (黄永丹),[1,2] Hua Qin (秦华),[1,a)] Baoshun Zhang (张宝顺),[1] Jingbo Wu (吴敬波),[3,b)] Gaochao Zhou (周高潮),[3] and Biaobing Jin (金飚兵)[3]
[1]*Key Laboratory of Nanodevices and Applications, Suzhou Institute of Nano-tech and Nano-bionics, Chinese Academy of Sciences, 398 Ruoshui Road, Suzhou, Jiangsu 215123, People's Republic of China*
[2]*University of Chinese Academy of Sciences, Beijing 100049, People's Republic of China*
[3]*Research Institute of Superconductor Electronics (RISE), School of Electronic Science and Engineering, Nanjing University, Nanjing 210093, People's Republic of China*

(Received 27 April 2013; accepted 4 June 2013; published online 27 June 2013)

Terahertz plasmon-polariton modes are excited and probed in a grating coupled GaN/AlGaN two-dimensional electron gas embedded in a Fabry-Pérot cavity using a terahertz time-domain spectroscopy at 8 K. A strong coupling between the plasmon modes and the cavity modes was observed. Electromagnetic simulations confirmed that both the cavity and the grating coupler play important roles in coupling the terahertz field and the plasmons. The finding suggests that the manipulation of terahertz plasmon-polariton could be achieved by engineering the Q-factor and the mode number of the cavity to further enhance the coupling strength. © *2013 AIP Publishing LLC*. [http://dx.doi.org/10.1063/1.4812359]

Two-dimensional plasmon, knowing as collective charge density oscillations in two-dimensional electron gas (2DEG), can be excited by external electromagnetic (EM) wave.[1] In 2DEGs formed in silicon metal-oxide-semiconductor field-effect transistors[2–4] or III-V heterostructures,[5–8] the plasmon frequency falls into the terahertz range of the EM spectrum and can be continuously tuned by varying the charge density in the range of 10^{11}–$10^{13}\,\mathrm{cm}^{-2}$ through the field effect. Plasmon in field-effect transistors has attracted strong interest for terahertz detectors,[9–13] emitters,[6,14–16] and modulators.[17] One of the key tasks to realize any of these devices is to achieve strong coupling between the terahertz EM wave and the plasmon. Metallic grating and antenna have been widely applied for this purpose.[2,4,8,10,18–21] A grating is an efficient coupler to feed EM wave into a large area 2DEG and excite two-dimensional (2D) plasmons or an ensemble of localized plasmons. However, the relatively short lifetime of plasmon in existing solid-state devices strongly limits the degrees of EM-wave and plasmon manipulation. Furthermore, a grating coupler is usually broadband and does not allow one to define a limited number of EM modes which is essential for strong interaction. A high-Q Fabry-Pérot cavity with a finite size can significantly reduce the mode number and enhance the terahertz electric field. Recently, plasmon excitation by near-field terahertz antennas/resonators as resonant EM cavities has been investigated towards the realization of plasmon-based terahertz devices.[20,22,23] In this letter, we report the observation of strong coupling between the plasmon modes and the cavity EM modes in a grating coupled 2DEG embedded in a Fabry-Pérot cavity using a terahertz time-domain spectroscopy (THz-TDS) at cryogenic temperature. Simulations on the local EM field agree well with the experimental results. An approach to further enhance the coupling by engineering the EM cavity is discussed.

The device contains two building blocks, namely, the grating-coupled 2DEG and the high-resistivity-float-zone silicon (HRFZ-Si) cap, as shown in Fig. 1. These two parts were bonded face-to-face to form a Sapphire/GaN/AlGaN/Vacuum/HRFZ-Si Fabry-Pérot cavity using the flip-chip bonding technique. The overall thickness of the Sapphire/GaN/AlGaN part is $D_1 = 190\,\mu\mathrm{m}$. The vacuum gap with $D_2 = 285\,\mu\mathrm{m}$ between the grating and the HRFZ-Si cap is introduced to avoid possible nonuniform surface stress or surface states. The effective thickness of the silicon layer is $D_3 = 250\,\mu\mathrm{m}$. The gold grating for coupling the terahertz EM wave to the 2DEG is fabricated on top of the GaN/AlGaN heterostructure and the 2DEG is about $d = 25\,\mathrm{nm}$ beneath the grating coupler. The grating has a period of $L = 4\,\mu\mathrm{m}$ and the individual gold finger has a length of $W = 2.7\,\mu\mathrm{m}$. The total area of the grating is set to be $4 \times 4\,\mathrm{mm}^2$ being slightly larger than the terahertz beam size. The electron mobility μ is about $2.0 \times 10^3\,\mathrm{cm}^2/\mathrm{Vs}$ at room temperature and about $1.5 \times 10^4\,\mathrm{cm}^2/\mathrm{Vs}$ at 8 K, respectively. The ungated 2DEG has an electron density about $1.0 \times 10^{13}\,\mathrm{cm}^{-2}$ at room temperature and approximately $1.2 \times 10^{13}\,\mathrm{cm}^{-2}$ at 77 K obtained from Hall measurements. The drain/source electrodes were connected to the ground and the grating was connected to a voltage source to tune the electron density underneath. The device was cooled down to 8 K in a liquid helium cryostat with two terahertz optical windows. The threshold voltage to deplete the 2DEG is $V_T = -3.9\,\mathrm{V}$. A standard THz-TDS setup[24,25] was applied for terahertz transmission measurement in which the terahertz electric field is perpendicular to the grating fingers, as schematically shown in Fig. 1.

The THz-TDS technique allows us to obtain the transmission spectrum at different gate voltages. From the time-domain signals shown in Figs. 2(a)–2(c), the difference between the device and the optical windows, and that

a)Author to whom correspondence should be addressed. Electronic mail: hqin2007@sinano.ac.cn
b)Present address: School of Electronic and Electrical Engineering, University of Leeds, Leeds LS2 9JT, United Kingdom.

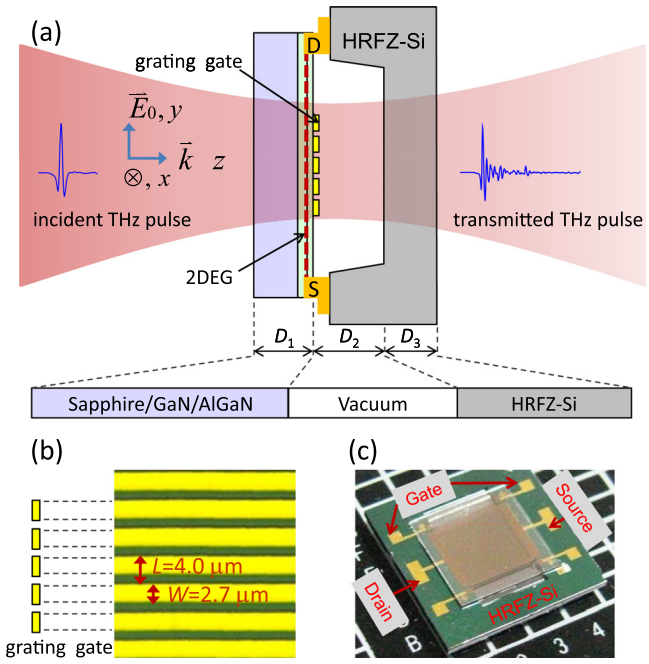

FIG. 1. (a) The Schematic cross-section of the device and the coordinate notation for transmission measurement. The optical micrographs of the grating gate (b) and the whole device (c).

between different gate voltages can already be clearly seen. By performing Fourier transformation of the time-domain signal and referencing to the signal without the device, the transmission spectra $T(V_G)$ can be obtained. As shown in Fig. 2(d), the transmission spectra at $V_G = 0\,\mathrm{V}$ and $V_G = -4.0\,\mathrm{V}$ display multiple peaks and clear variations in different frequency ranges. The multiple peaks are fundamental modes (C_1–C_{13}) of the Fabry-Pérot cavity and are well reproduced by simulations using the finite-difference time domain (FDTD) method and the transferring matrix (TM) technique, as shown in Fig. 2(e). The effect of the gate-controlled 2DEG on the terahertz transmission ($T(V_G)/T(V_G < V_T)$) can be obtained by normalizing the corresponding transmission spectrum by the transmission spectrum in the pinch-off state ($V_G = -4.0\,\mathrm{V}$). In Fig. 2(f), the spectrum $T(0\,\mathrm{V})/T(-4.0\,\mathrm{V})$ exhibits a strong resonance (C_7) around 0.797 THz among other relatively weaker resonances. By varying the gate voltage from $-4.0\,\mathrm{V}$ to $0\,\mathrm{V}$ in a step of $0.1\,\mathrm{V}$, both the direct-current (DC) source-drain conductance (Fig. 3(a)) and the gate-voltage-controlled transmission spectra were measured. By mapping the gate-voltage-controlled transmission spectra into a color-scale plot, not only the resonant transmission peaks from the Fabry-Pérot cavity but also the resonant absorption lines from four plasmon modes can be seen in Fig. 3(b).

A 2DEG supports plasmon modes in a broad frequency range according to the dispersion relation[1]

$$\omega_p = 2\pi f_p = \sqrt{\frac{n_s e^2}{2m^*\varepsilon_0\bar{\varepsilon}}}\,q, \tag{1}$$

where ω_p and q are the plasmon frequency and wave vector, n_s is the electron density, e is the electron charge, $m^* = 0.2m_0$ is the effective electron mass with m_0 as the free electron mass, ε_0 and $\bar{\varepsilon}$ are the vacuum dielectric permittivity and effective dielectric constant. In the case of 2D plasmons excited, the plasmon wave vector is determined by $q_m = 2m\pi/L$ with $m = 1, 2, 3, \ldots$.[2,4] On the other hand, when localized plasmons are excited under the grating fingers, the wave vector is determined by $q_m = m\pi/W$.[18,21] In the fully screened case, i.e., the heterostructure surface is completely covered by metal, the effective dielectric constant is $\bar{\varepsilon}_{\mathrm{screened}} = [\varepsilon_1 + \varepsilon_2 \coth(qd)]/2$, where $\varepsilon_1 = 9.7$ and $\varepsilon_2 = 9.5$ are the dielectric constants of the GaN layer and AlGaN layer, respectively.[26] In the unscreened/open case, i.e., the heterostructure surface is open to a vacuum, the effective dielectric constant is $\bar{\varepsilon}_{\mathrm{open}} = [\varepsilon_1 + \varepsilon_2 \frac{1+\varepsilon_2\tanh(qd)}{\varepsilon_2+\tanh(qd)}]/2$.[27] By fitting the dispersion curves for both localized (as shown in Fig. 4(a)) and 2D (not shown) plasmon models to the plasmon frequencies extracted at $V_G = -0.3, -2.2\,\mathrm{V}$, we found the localized plasmon modes are more appropriate.[28] These two specific gate voltages was chosen since the corresponding plasmon modes are decoupled from the cavity. In the fitting, the electron density was set as $1.1 \times 10^{13}\,\mathrm{cm}^{-2}$ for

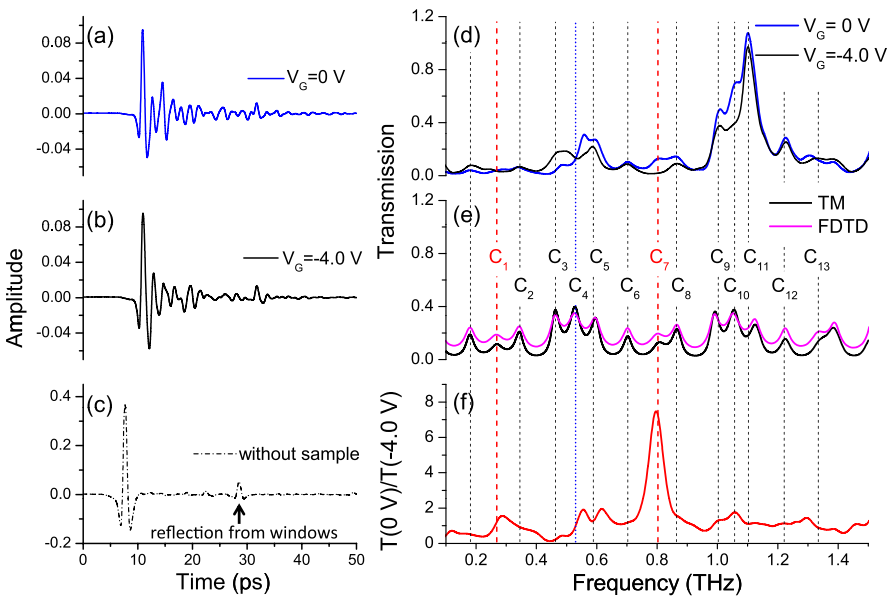

FIG. 2. The temporal transmitted terahertz field with the device at $V_G = 0\,\mathrm{V}$ (a), $V_G = -4.0\,\mathrm{V}$ (b), and without the device (c). (d) The transmission spectra of the device at $V_G = 0, -4.0\,\mathrm{V}$. (e) The simulated transmission spectra of the Sapphire/AlGaN/GaN/Vacuum/HRFZ-Si Fabry-Pérot cavity. (f) The transmission spectrum at $V_G = 0\,\mathrm{V}$ taking that at $V_G = -4.0\,\mathrm{V}$ as a reference.

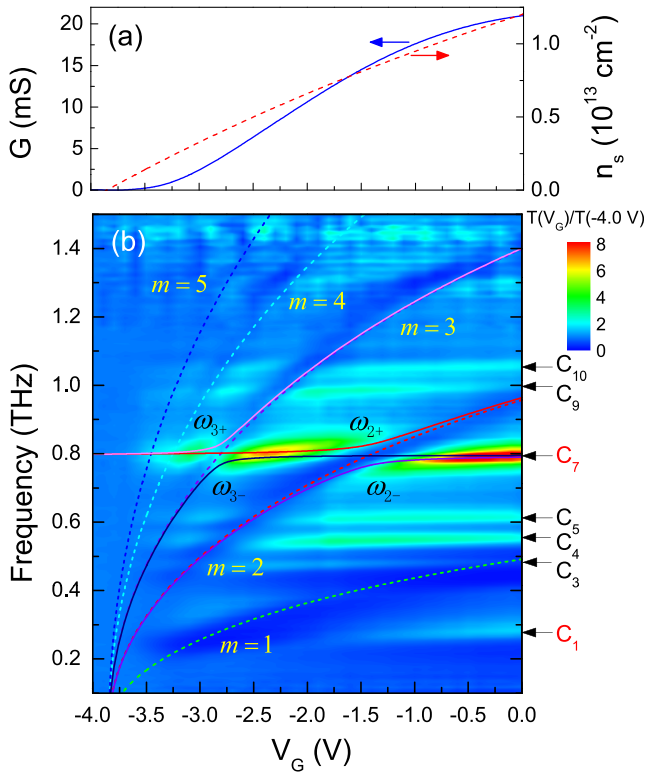

FIG. 3. (a) The measured DC drain-source conductance and the deduced electron density as a function of the gate voltage. (b) The transmission spectra taken at different gate voltage at 8 K. Dashed lines are localized plasmon modes ($m = 1, 2, \ldots, 5$) calculated based on Eq. (1). Solid lines are plasmon-polariton modes calculated from the cavity mode C_7 and the plasmon modes ($m = 2$ at $V_G = -1.4$ V, $m = 3$ at $V_G = -2.8$ V) based on Eq. (2).

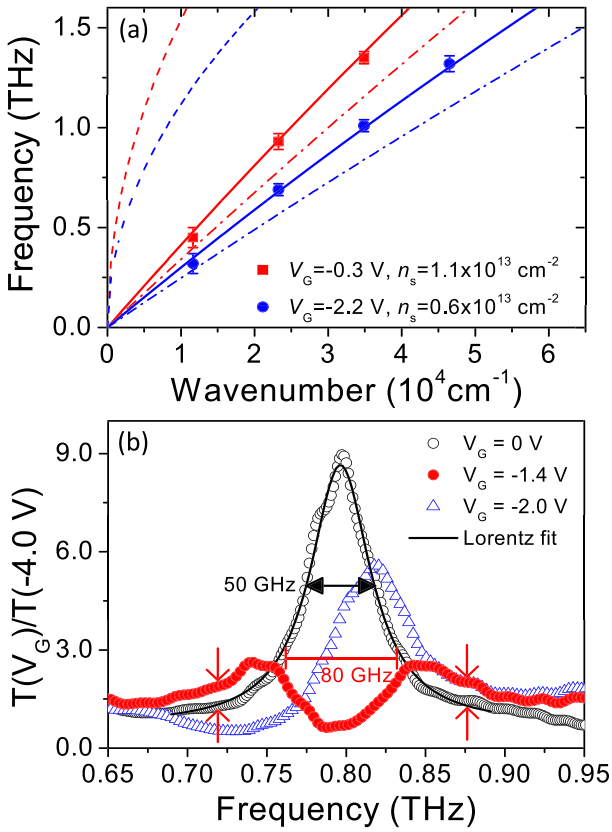

FIG. 4. (a) The red/blue curves are dispersion relations calculated for localized plasmons at $V_G = -0.3$ V ($n_s = 1.1 \times 10^{13}$ cm^{-2}) and $V_G = -2.2$ V ($n_s = 0.6 \times 10^{13}$ cm^{-2}), respectively. The dashed, dashed-dotted, and solid curves are for the unscreened, fully screened, and partially screened surface, respectively. The frequencies of the observed localized plasmons ($m = 1, 2, 3, 4$) at $V_G = -0.3/-2.2$ V are plotted as red/blue symbols. (b) Transmission spectra around 0.797 THz (C_7) with $V_G = 0$ V, -1.4 V, and -2.0 V, corresponding to $\omega_p > \omega_c$, $\omega_p = \omega_c$, and $\omega_p \lesssim \omega_c$.

$V_G = -0.3$ V and 0.6×10^{13} cm^{-2} for $V_G = -2.2$ V. The experiment data points for each electron density fall in between the corresponding unscreened (dashed lines) and the fully screened (dashed-dotted lines) dispersion curves, as shown in Fig. 4(a). Furthermore, it is found that the dispersion curves (solid lines) fit well to the experiment when the effective dielectric constant is approximated by the geometrical average of the dielectric constants for the gated and ungated 2DEG areas. All of the plasmon modes observed in Fig. 3(b) are well fitted by the calculated dispersion curves (dashed lines) based on the localized plasmon model and the averaged effective dielectric constant. It is more likely that an ensemble of localized plasmons confined by individual grating fingers is excited in our device. However, it is worth mentioning that the deduced effective electron density at terahertz frequency, as shown in Fig. 3(a), is close to but evidently different from the electron density in DC limit.[4,5]

As shown in Fig. 3(b), the resonant transmission peak C_7 splits into two lower branches (ω_{2-}, ω_{3-}) and two upper branches (ω_{2+}, ω_{3+}) when it is intersected with the resonant plasmon absorption lines ($m = 2$ and $m = 3$). The lower and upper branches are plasmon-polariton modes formed in the resonant coupling regime. The bare cavity mode C_7 at $V_G = 0$ V and its Lorentzian line shape are compared to the cavity modes at $V_G = -1.4$ V and $V_G = -2.0$ V, corresponding to a zero ($\omega_p = \omega_c$, $\omega_c = 2\pi f_c$ is the angular frequency of cavity mode) and a non-zero ($\omega_p \lesssim \omega_c$) detuning with plasmon mode $m = 2$, respectively, in Fig. 4(b). Following the coupled oscillator model, the plasmon-polariton frequency can be written as[29]

$$\omega_{\pm} = \frac{\omega_c + \omega_p}{2} - \frac{i}{2}(\gamma_c + \gamma_p) \pm \sqrt{\left(\frac{\omega_c - \omega_p}{2}\right)^2 + V^2 - \left(\frac{\gamma_c - \gamma_p}{2}\right)^2 + \frac{i}{2}(\gamma_c - \gamma_p)(\omega_p - \omega_c)}. \quad (2)$$

The linewidths of the cavity mode ($\gamma_c/2\pi = 50$ GHz) and the plasmon mode ($\gamma_p/2\pi = 80$ GHz) can be directly extracted from the transmission spectra. The corresponding Q-factors at $f_c = 0.797$ THz are $Q_c = 2\pi f_c/\gamma_c = 16$ and $Q_p = 2\pi f_p/\gamma_p = 10$. Assuming a coupling strength of $V/2\pi = 35$ GHz, the calculated plasmon-polariton modes

agree well with the mode splitting shown in Fig. 3(b). The resulting Rabi oscillation has a frequency of $\Omega_R = \omega_{2+} - \omega_{2-} = \sqrt{4V^2 - (\gamma_c - \gamma_p)^2} = 2\pi \times 63\,\text{GHz}$.

It is the strong field enhancement by the grating gate and the small mode volume that enables the strong coupling and the formation of plasmon-polaritons. To illustrate the coupling between the cavity mode and the plasmon mode, we performed a FDTD simulation on the EM cavity modes and the corresponding field distribution. In the simulation, the exact device dimensions and the grating gates were considered. However, the thin layers of the GaN/AlGaN heterostructure and the 2DEG layer were omitted to simplify the simulation. The longitudinal terahertz field strength ($|E_y|$) seen by the 2DEG at the midpoint of the ungated channel segment as a function of the incident terahertz frequency is shown in Fig. 5(a). Strong resonances (C_1, C_7, and C_{13}) at 0.266 THz, 0.797 THz, and 1.329 THz among other resonances are identified and are in consistent with the overall transmission spectra shown in Figs. 2(d), 2(e), and 3(b). The spatial distributions of the terahertz field within the Fabry-Pérot cavity are extracted for resonance C_1 and C_7 as shown in Figs. 5(b) and 5(c), respectively. Resonances C_1, C_4, C_7, C_{10}, and C_{13} correspond to the 1st, 2nd, 3rd, 4th, and 5th cavity modes ($nD_1 = \lambda/2$, λ, $3\lambda/2$, 2λ, and $5\lambda/2$, with $n = 3.0$ as the refractive index of sapphire). At these resonances, the local terahertz field seen by the 2DEG close to the edges of the grating fingers is further enhanced by a factor of 4 by the grating gates. This field enhancement gives rise to the strong coupling between the cavity mode and the plasmon mode, which is analogous to the strong coupling between the terahertz metamaterial resonator and the electron cyclotron transition in quantum wells induced by the strongly enhanced evanescent field of the metamaterial resonant mode.[22] To achieve an even stronger coupling, two aspects of the Fabry-Pérot cavity can be engineered. First, the Q-factor of the cavity can be improved by rendering two reflective mirrors to the cavity ports rather than having two open surfaces in current study. Technically, two semi-transparent layers of superconducting NbN film could serve as high-reflectivity and low-loss terahertz mirrors.[30] Second, the cavity size can be kept as small as possible to reduce the mode number. To this end, the thickness of sapphire substrate, the vacuum gap and the thickness of the HRFZ-Si cap should be optimized to support the resonant cavity modes. By replacing the vacuum gap and the HRFZ-Si cap with a sapphire plate, a more symmetric Fabry-Pérot cavity could be realized.

In conclusion, we embedded a grating-coupled GaN/AlGaN 2DEG structure in a Fabry-Pérot cavity. Four plasmon modes were resonantly excited and probed by using a THz-TDS technique at 8 K. A strong plasmon-cavity mode coupling and the resulting plasmon-polariton were observed and analyzed. FDTD simulations revealed that both the Fabry-Pérot cavity and the grating coupler are essential for coupling and manipulating the local terahertz field and the plasmons. An even stronger coupling to create and manipulate terahertz plasmon-polaritons could be realized by improving the Q-factor and reducing the mode number of the cavity.

The authors acknowledge the support from the National Basic Research Program of China (G2009CB929303), and the Knowledge Innovation Program of the Chinese Academy of Sciences (Y0BAQ31001 and KJCX2-EW-705). This work was also partially supported by the CAEP THz Science and Technology Foundation under the Grant No. CAEPTHZ201205. H.Q. thanks the insightful discussion with Jörg P. Kotthaus on plasmon excitation.

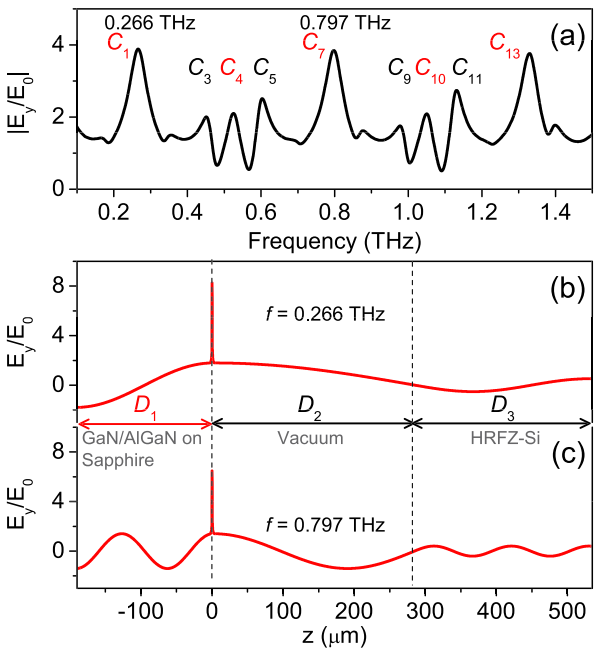

FIG. 5. (a) The longitudinal terahertz field strength $|E_y|$ at the midpoint of the ungated channel segment as a function of the incident terahertz frequency. Spatial distribution of E_y at (b) 0.266 THz and (c) 0.797 THz. The fields are all normalized to the incident field E_0.

[1]F. Stern, Phys. Rev. Lett. **18**, 546 (1967).
[2]S. J. Allen, D. C. Tsui, and R. A. Logan, Phys. Rev. Lett. **38**, 980 (1977).
[3]T. N. Theis, J. P. Kotthaus, and P. J. Stiles, Solid State Commun. **26**, 603 (1978).
[4]U. Mackens, D. Heitmann, L. Prager, J. P. Kotthaus, and W. Beinvogl, Phys. Rev. Lett. **53**, 1485 (1984).
[5]E. Batke, D. Heitmann, J. P. Kotthaus, and K. Ploog, Phys. Rev. Lett. **54**, 2367 (1985).
[6]K. Hirakawa, K. Yamanaka, M. Grayson, and D. C. Tsui, Appl. Phys. Lett. **67**, 2326 (1995).
[7]I. V. Kukushkin, D. V. Kulakovskiĭ, S. A. Mikhaĭlov, J. H. Smet, and K. von Klitzing, JETP Lett. **77**, 497 (2003).
[8]A. V. Muravjov, D. B. Veksler, V. V. Popov, O. V. Polischuk, N. Pala, X. Hu, R. Gaska, H. Saxena, R. E. Peale, and M. S. Shur, Appl. Phys. Lett. **96**, 042105 (2010).
[9]M. I. Dyakonov and M. S. Shur, IEEE Trans. Electron Devices **43**, 380 (1996).
[10]E. A. Shaner, M. Lee, M. C. Wanke, A. D. Grine, J. L. Reno, and S. J. Allen, Appl. Phys. Lett. **87**, 193507 (2005).
[11]F. Teppe, W. Knap, D. Veksler, M. S. Shur, A. P. Dmitriev, V. Yu. Kachorovskii, and S. Rumyantsev, Appl. Phys. Lett. **87**, 052107 (2005).
[12]V. V. Popov, D. V. Fateev, T. Otsuji, Y. M. Meziani, D. Coquillat, and W. Knap, Appl. Phys. Lett. **99**, 243504 (2011).
[13]G. C. Dyer, S. Preu, G. R. Aizin, J. Mikalopas, A. D. Grine, J. L. Reno, J. M. Hensley, N. Q. Vinh, A. C. Gossard, M. S. Sherwin, S. J. Allen, and E. A. Shaner, Appl. Phys. Lett. **100**, 083506 (2012).
[14]D. C. Tsui, E. Gornik, and R. A. Logan, Solid State Commun. **35**, 875 (1980).
[15]M. Dyakonov and M. Shur, Phys. Rev. Lett. **71**, 2465 (1993).
[16]S. Boubanga-Tombet, F. Teppe, J. Torres, A. El Moutaouakil, D. Coquillat, N. Dyakonova, C. Consejo, P. Arcade, P. Nouvel, H. Marinchio, T. Laurent,

C. Palermo, A. Penarier, T. Otsuji, L. Varani, and W. Knap, Appl. Phys. Lett. **97**, 262108 (2010).
[17]K. Nogajewski, J. Lusakowski, W. Knap, V. V. Popov, F. Teppe, S. L. Rumyantsev, and M. S. Shur, Appl. Phys. Lett. **99**, 213501 (2011).
[18]A. R. Davoyan, V. V. Popov, and S. A. Nikitov, Phys. Rev. Lett. **108**, 127401 (2012).
[19]G. C. Dyer, N. Q. Vinh, S. J. Allen, G. R. Aizin, J. Mikalopas, J. L. Reno, and E. A. Shaner, Appl. Phys. Lett. **97**, 193507 (2010).
[20]G. C. Dyer, G. R. Aizin, S. Preu, N. Q. Vinh, S. J. Allen, J. L. Reno, and E. A. Shaner, Phys. Rev. Lett. **109**, 126803 (2012).
[21]G. R. Aizin and G. C. Dyer, Phys. Rev. B **86**, 235316 (2012).
[22]G. Scalari, C. Maissen, D. Turčinková, D. Hagenmüller, S. De Liberato, C. Ciuti, C. Reichl, D. Schuh, W. Wegscheider, M. Beck, and J. Faist, Science **335**, 1323 (2012).
[23]D. Dietze, K. Unterrainer, and J. Darmo, Phys. Rev. B **87**, 075324 (2013).
[24]J. B. Wu, B. B. Jin, J. Wan, L. J. Laing, Y. G. Zhang, T. Jia, C. H. Cao, L. Kang, W. W. Xu, J. Chen, and P. H. Wu, Appl. Phys. Lett. **99**, 161113 (2011).
[25]B. Ferguson and X. C. Zhang, Nature Mater. **1**, 26 (2002).
[26]A. V. Chaplik, Sov. Phys. JETP **35**, 395 (1972) [Zh. Eksp. Teor. Fiz. **62**, 746 (1972)].
[27]D. V. Fateev, V. V. Popov, and M. S. Shur, Semiconductors **44**, 1406 (2010).
[28]An unreasonablely low charge density ($\approx 0.6 \times 10^{13}$ cm^{-2}) at $V_G = -0.3$ V is required to give a good fit to the experiment data points if a 2D plasmon mode is assumed.
[29]A. Kavokin, J. Baumberg, G. Malpuech, and F. Laussy, *Microcavities* (Oxford University Press, 2007).
[30]L. Kang, B. B. Jin, X. Y. Liu, X. Q. Jia, J. Chen, Z. M. Ji, W. W. Xu, P. H. Wu, S. B. Mi, A. Pimenov, Y. J. Wu, and B. G. Wang, J. Appl. Phys. **109**, 033908 (2011).